The Journal of Chemical Physics

Rheological properties of super critical CO_2 with CuO: Multi-scale computational modeling

Cite as: J. Chem. Phys. **149**, 224702 (2018); https://doi.org/10.1063/1.5053571
Submitted: 23 August 2018 . Accepted: 22 November 2018 . Published Online: 11 December 2018

Rasoul Khaledialidusti, Abhishek Kumar Mishra, and Afrooz Barnoush

AIP Publishing

Rheological properties of super critical CO_2 with CuO: Multi-scale computational modeling

Rasoul Khaledialidusti,[1,a)] Abhishek Kumar Mishra,[2,a)] and Afrooz Barnoush[1,a)]
[1]*Department of Mechanical and Industrial Engineering, NTNU, Trondheim, Norway*
[2]*Physics Department, School of Engineering Science, University of Petroleum and Energy Studies, Dehradun 248007, India*

(Received 23 August 2018; accepted 22 November 2018; published online 11 December 2018)

A multi-scale computational methodology based on the density functional theory and molecular dynamics has been used to investigate the rheological properties of super critical CO_2 with CuO nano-particle (NP). Density functional theory which treats the electron density as the central variable has been used to explore the adsorption of CO_2 molecules on the two most stable CuO surfaces [i.e., (111) and (011)] at absolute zero. The results of this theory would provide valuable information to make CuO NPs with the surface where the CO_2 adsorption is maximum in order to have a stronger mono-layer of adsorbed CO_2 molecules on the surface of the NP which is the most crucial factor in formation of a stable nanofluid. The results show that the CO_2 molecule is adsorbed more strongly on the (011) surface with an adsorption energy of −99.06 kJ/mol compared to the (111) surface. A computational methodology based on molecular dynamics has been used to evaluate the enhancement of the rheological properties of the super-critical CO_2 liquid based nanofluid at different temperatures and pressures. In this scale, first, the CO_2 liquid has been modeled by employing the condensed-phase optimized molecular potentials for atomistic simulation studies (COMPASS) force field potential and the fluid properties computed are in excellent agreement with the literature and experiment values. Second, the nanofluid has been modeled in order to study the enhancement of the fluid properties with the CuO NPs. The charged optimized many-body force field potential has been employed to consider the effect of the charge transferring between the NPs and liquid molecules and breaking of existing bonds and the formation of new bonds. The COMPASS force field potential is also employed for the interactions between CO_2 molecules. The combination of these potentials is quite a new approach for the study of the super-critical (SC)-CO_2 based nanofluid. The results show that the viscosity of the SC-CO_2 is enhanced between 1.3 and 2.5 times under the temperature and pressure conditions studied. *Published by AIP Publishing.* https://doi.org/10.1063/1.5053571

I. INTRODUCTION AND BACKGROUND

Enhancement of rheological properties of different kinds of fluids has gained considerable attention in recent years.[1–6] Nano-particles (NPs) are introduced as a useful element for this purpose to enhance thermo-physical, chemical, rheological, and physiochemical fluid properties.

There are different applications for the enhancement of fluid properties with NPs in lubrication,[7] biological,[8] oil and gas,[9] and chemical industries.[10] For example, in the energy-based system, the viscosity of the fluid plays an important role for heat transfer and fluid transport. The higher viscosities of the fluid provide an excellent condition in dissipating heat in the coolant systems. The other example is related to the super-critical (SC) CO_2 liquid injection in oil reservoirs which results in lower CO_2 mobility that could reduce problems with poor macroscopic sweep efficiency in the oil reservoirs. Therefore, the design of an economic CO_2 thickener remains an extremely relevant research topic for CO_2-Enhanced Oil Recovery (EOR). Besides their high cost, the efficiency of thickeners such as polymers, foams, and gels is not satisfactory due to the long-term stability which is difficult to maintain. The use of NPs instead of surfactants to stabilize CO_2 by forming a nanofluid may overcome the long-term instability and surfactant adsorption loss and high cost issues that affect the efficiency of CO_2-EOR processes.

Nanofluids are mainly characterized by the fact that Brownian agitation overwhelms any settling motion due to gravity. Undesirably, particle collision can lead to the agglomeration process so that particles up to micron-size are produced. Due to their weight, such particles cannot be maintained in suspension by Brownian agitation and they settle out of suspension. However, if the particles have a sufficient high repulsion, the suspensions will exist in a stable state. Thus, a stable nanofluid is possible as long as the van der Waals (vdW) interactions between the NPs are decreased. For stable nanofluids, the repulsive forces between the particles must be dominant and this would be provided by a stronger mono-layer of adsorbed CO_2 molecules on the surface of the NP which is the most crucial factor in the formation of a stable nanofluid.

[a)]Authors to whom correspondence should be addressed: rasoul.khaledialidusti@ntnu.no; mishra_lu@hotmail.com; and afrooz.barnoush@ntnu.no

Evaluating the thickening of CO_2 using NPs and forming a CO_2 based nanofluid which might have more appropriate rheological properties is challenging. The choice of the appropriate NP composition in which the CO_2 molecules are attached more strongly on the NP surface is the most crucial point in realizing this vision.

The experimental investigation of the SC CO_2 liquid based nanofluid requires high pressure equipment that makes these analyses very expensive. Therefore, the multi-scale computational modeling of such systems would provide a great opportunity to study the different fluid properties (e.g., viscosity) at very low and high pressures and temperatures that could not be tested before.

In order to understand the physics behind the NP surface interaction with fluid molecules, it is necessary to study the system at the atomic scale, where the size is in the order of nanometers (nm). Quantum mechanics (QM) equations of the electronic structure, the so-called *ab initio* calculations, are the most accurate of all molecular modeling approaches to study the interaction of fluid molecules with the solid surfaces. This approach is based on the solution of Schrödinger's wave equation which requires no empirical and previous experimental parameters. However, even the best QM modeling methods [i.e., Density Functional Theory (DFT)] are limited to around 10^3 atoms and to dynamics simulations of a few picoseconds. Molecular Dynamics (MD) modeling might pose the limitation of the DFT approach by modeling the motion of a system of particles with respect to the forces that are obtained from DFT calculations. These methodologies are not as simple as they seem and they require a deep understanding of the theories behind them and of the physiochemical interactions with thermo-physical boundary conditions. There are a lot of algorithms and mathematical models that must be considered in order to model the accurate behavior of the systems.

In this study, we use *ab initio*–quantum mechanics guided nanoparticle selection combined with atomistic simulation for calculating the rheological properties of the nanofluid. We study the interactions of CO_2 molecules with different CuO surfaces by solving the quantum mechanics equations of the electronic structure. *Ab initio* QM has been employed to investigate the role of crystal orientations of CuO on the CO_2 chemisorption energy in order to find the orientation where the CO_2 adsorption is stronger. This will reveal the most promising CuO surface for the NP to make the CO_2 based nanofluid. Then, the cylindrical NP has been modeled with the cross sections, which provide the surface that has the stronger chemisorption energy. Further atomistic simulations of liquid CO_2 interactions with nanoparticles with the most promising surface will be performed using MD methods to study the rheological SC-CO_2 based nanofluid properties at different thermodynamic states. The results from *ab initio* QM would be helpful to make a nanofluid with a stronger mono-layer of adsorbed CO_2 molecules on the surface of the NP, which is the most crucial factor in formation of a stable nanofluid.

For MD modeling, the condensed-phase optimized molecular potentials for atomistic simulation studies (COMPASS) force field[11] has been employed for the CO_2 molecules and the charged optimized many body (COMB) force field[12,13] has been employed for the CuO NP and CO_2 molecule interactions, in which the parameters are well determined based on the *ab initio* QM calculations. The surface energies, thermal properties, and defect formation enthalpies are also in good agreement with the *ab initio* QM calculations. These potentials would provide a great possibility to take the effect of the multiple oxidation states of Cu in a metal oxide bond formation. They would also provide a way to capture the effect of the flexibility for changing the state of metal-metal and metal-oxide bonds during the interaction. Therefore, compared to previous studies, applying these potentials would mimic a more realistic and reasonable condition for the base SC-CO_2 fluid including CuO NP.

Various studies were performed for the simulation of the nanofluid; however, most of the studies were applied for studying the NP dispersion in an inert fluid (i.e., argon)[1–4] and water[5] and with different common force fields used in MD simulations such as Lennard-Jones (L-J),[14] Buckingham,[15] Embedded-Atom method (EAM),[16] Tersoff,[17] and Reactive Empirical Bond Order (REBO).[18] For example, Sankar *et al.*[2] and Li *et al.*[1] investigated a nanofluid system including the Cu NP with the base fluid of argon by the help of EAM and L-J potentials. Rudyak and Krasnolutskii[4] carried out work on aluminum and lithium NPs with liquid argon using the L-J potential and they showed the effect of the size and material of the NP on the viscosity. Loya and Ren[5] worked on the rheological properties of water including CuO NP; however, the COMB potential was applied rather than the commonly used MD force fields. Rudyak and Minakov[6] studied the viscosity, thermal conductivity, and heat transfer properties of nanofluids using the L-J potential.

The objective of the present study is the enhancement of the thickening of SC-CO_2 using the CuO NPs and forming a CO_2 based nanofluid which can improve, for example, the volumetric sweep efficiency compared to conventional CO_2-EOR methods in the oil reservoirs or the efficiency of the energy-based systems for other applications.

II. COMPUTATIONAL METHODOLOGY

A. *Ab initio* QM (DFT) modeling

Spin-polarized periodic DFT calculations have been performed using the Vienna *Ab initio* Simulation Package (VASP) with a plane-wave basis set[19–22] to find the highest chemisorption energy of the CO_2 molecule on the different CuO surfaces at absolute zero. The DFT+U[23] methodology and the formalism of Dudarev *et al.*[23] have been employed since this methodology with an appropriate U can accurately describe the CuO structure. The exchange-correlation effects have been described within the generalized gradient approximation (GGA) using the functional of Perdew, Burke, and Ernzerhof (PBE).[24,25] The U_{eff} value is selected for the localized 3d electrons of Cu, where $U_{eff} = U - J$, i.e., the difference between the Coulomb U and exchange J parameters. To optimize the geometry, a conjugate gradients' technique has been applied with an iterative relaxation of the atomic positions with the residual forces acting on the atoms of 0.01 eV/Å and a total energy convergence of 10^{-5} eV per unit cell. A very small Fermi

smearing of 0.01 has been employed for this semiconductor (i.e., CuO) and the CO_2 molecule since the extrapolation of the total energy to absolute zero is only valid for metals with a continuous density of states (DOS) at the Fermi level.[26]

Chemisorption energy of CO_2 onto different CuO orientation has been calculated as follows:

1. Optimizing bulk structure (i.e., CuO)

In order to obtain the best match of the bulk structure with the experiments, first, the unit cell geometry has been created by the Atomic Simulation Environment (ASE),[27] as shown in Fig. 1. Atomic structures for DFT calculations have been visualized using Visualization for Electronic and STructural Analysis (VESTA).[28]

Then, different planewave cutoff energies and k-point grids have been tested to reach the total energy convergence of 1 meV. The results are shown in Appendix A. Based on the results obtained, an energy cutoff of 500 eV has been employed and the Brillouin zone has been sampled using a $9 \times 9 \times 9$ Monkhorst-Pack[29] k-point mesh for the primitive cells of CuO. These dense grids and the energy cutoff for the plane-wave basis set ensured an accurate description of properties that are influenced by sharp features in the density of states. This plane-wave cutoff has been kept constant for all the calculations; however, the number of k-points has been varied with the size of the unit cell.

The CO_2 adsorption on copper oxide has been investigated extensively using DFT based techniques.[30–33] In this study, in order to find the best match of the bulk unit cell with the experiments, different U_{eff} have been tested and the lattice parameters, magnetic moments (μ_B), and bandgap (E_g) values have been compared with the experimental values (Table I). Total DOS with different U_{eff} are shown in Fig. 2. As can be seen, at U_{eff} = 0 eV, there is no bandgap and the DOS is smeared across the Fermi level with no magnetic states on the Cu atoms; however, in semiconductors, there must be an energy gap between the occupied and unoccupied states. The results show that both the bandgap and the magnetic moment are increased with the U_{eff} values and the best agreement with the experimental values is obtained at the U_{eff} = 7 eV. It is worth noting that U_{eff} = 7 eV not only reproduces an accurate bandgap and magnetic moment for CuO but also results in a good match of structural parameters.[34–37] Our results are in reasonable agreement with the previous work of Mishra *et al.*[34] and Nolan and Elliott,[38] where they evaluated the effect of the U_{eff} value on Cu–O distances, magnetic moments, and bandgaps. Ekuma *et al.*[39] suggested a U_{eff} value of 7.14 eV using the PBE+U methodology; we repeated our calculations with this suggested U_{eff} value, but no substantial modifications were detected in any of the parameters.

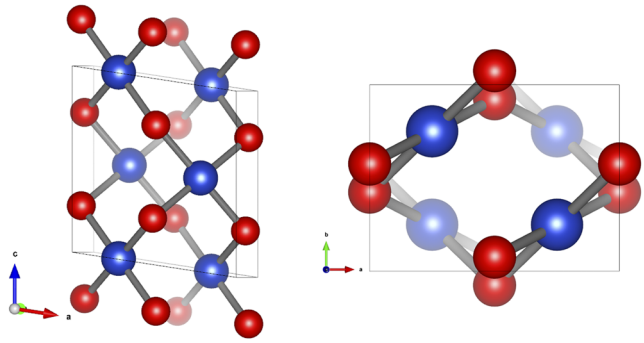

FIG. 1. A schematic of CuO bulk structure in side view (left) and top view (right). Blue and red spheres represent Cu and O atoms, respectively.

2. Relaxing surface

After optimizing the bulk structure, the surface cell has been cleaved with enough layers to get bulk properties of the adsorbent (i.e., CuO), and a vacuum slab large enough to accommodate the adsorbate molecules (i.e., CO_2) has been added. Different slabs, vacuum thickness, and a number of relaxed layers have been tested to reach the energy convergence of 1 meV. The energy is converged with a $5 \times 5 \times 1$ Monkhorst-Pack[29] k-point mesh for the (1×1) surface cells including a slab of four layers with the uppermost two layers free to move while the two bottom layers has been kept fixed at the bulk geometry. The cell dimensions have also been fixed. The vacuum region of 15 Å above the surface has been considered which is large enough to avoid interactions between the periodic slabs. [There are 16 Cu and 16 O atoms in a (1×1) surface slab.]

In order to evaluate the highest chemisorption energy of the CO_2 molecule on the CuO surfaces, two different most stable, low index CuO surfaces [i.e., (111) and (011)] have been focused. Three different possible magnetic orderings of the atoms in the surfaces (i.e., bulk-like, line-by-line, and layer-by-layer) have been investigated, and the energy of the optimized surfaces (E_{surf}) has been calculated.

The bonding distance and atomic arrangements of the surface structures have been changed after relaxation. Figure 3 shows the (011) and (111) CuO surface structures after

TABLE I. Lattice parameters (a, b, c, and β), Cu–O and O–O distances (d_{Cu-O} and d_{O-O}), bandgap (E_g), and magnetic moment (m_s) for CuO bulk: comparing the calculated quantities by DFT+U at different U_{eff} values with experimental results.

U_{eff} (eV)	a (Å)	B (Å)	C (Å)	β (deg)	d_{cu-O} (Å)	d_{O-O} (Å)	E_g (eV)	m_s (μ_B)
0	4.5961	3.4647	5.1005	100.21	1.921	2.602	...	0
3	4.6393	3.4231	5.1051	99.61	1.937	2.609	0.45	0.53
5	4.6523	3.4111	5.1041	99.29	1.949	2.609	0.96	0.61
7	4.6627	3.4095	5.0978	99.48	1.948	2.612	1.53	0.67
9	4.6829	3.3879	5.1036	99.17	1.950	2.615	2.22	0.73
Experiment[34–37]	4.6837	3.4226	5.1288	99.54	1.951	2.625	1.4–1.7	0.65–0.69

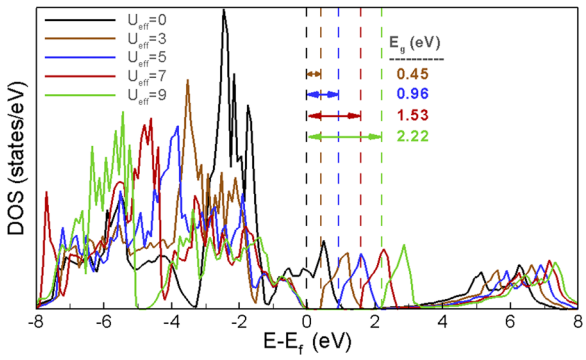

FIG. 2. Total density of states of CuO with DFT+U. Black perpendicular dashed line shows the Fermi energy, and the distance between the other dashed lines and Fermi energy shows the bandgap at different U_{eff} values.

relaxations. In this figure, a (2 × 2) supercell structure has been illustrated in order to visualize the bonding and atomic arrangement in a more clear way.

3. Optimizing complete system (adsorbate and adsorbent)

After calculating the surface energy, the adsorbate molecule (i.e., CO_2) has been added on top of the surfaces. Then, the geometry has been optimized, and the energy of the optimized geometry ($E_{surf+mol}$) has been calculated. As shown in Fig. 4, the top layer of the surfaces consists of different atomic sites (O and Cu). The energy has been evaluated by placing the CO_2 molecule on top of these sites parallel and perpendicularly with different orientations of the CO_2 molecule in order to find the lowest energy which is the most possible place to adsorb the CO_2 molecule. Symmetry constraints have not been applied in the optimization; in particular, the CO_2 molecule allows reorienting and moving freely away laterally and vertically from the initial site to find the minimum energy adsorption structure.

Long-range dispersion forces have been taken into account with the electron correlations for the long-range interactions (DFT-D2) method of Grimme[40] that are responsible for van der Waals (vdW, dispersive) forces and are required for the accurate description of the interactions between the CO_2 molecule and CuO surfaces. The CO_2 molecule freely moves in all directions and reorients to reach the minimum energy adsorption.

The CO_2 adsorption has been studied on a (2×2) supercell in the two surfaces in order to avoid the interaction between neighboring CO_2 molecules due to the periodic condition. In order to illustrate the point, one of the configurations of CO_2 adsorption on the (011) CuO surface, as an example, is shown in Fig. 4. The other configurations are explained in detail in the following.

4. Optimizing adsorbate molecule

In order to calculate the energy of the free adsorbate (i.e., CO_2) molecule, the adsorbent (i.e., CuO) surface has been removed and the isolated molecule has been optimized in the same cell, sampling only the gamma-point of the Brillouin zone with the same parameters described for the surfaces. Then, the energy of the optimized system (E_{mol}) has been calculated.

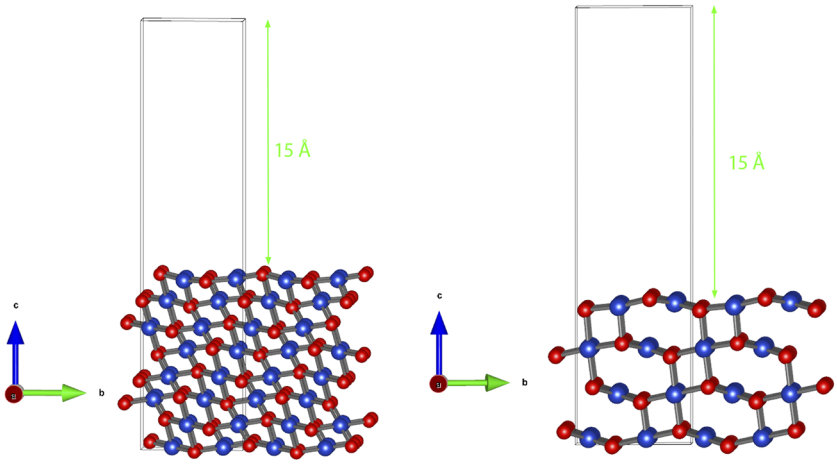

FIG. 3. Representation of the side view for the relaxed CuO surfaces and the slab vacuum. A (2×2) supercell is shown for a clear visualization. Left: CuO(011); right: CuO(111). Blue and red spheres represent Cu and O atoms, respectively.

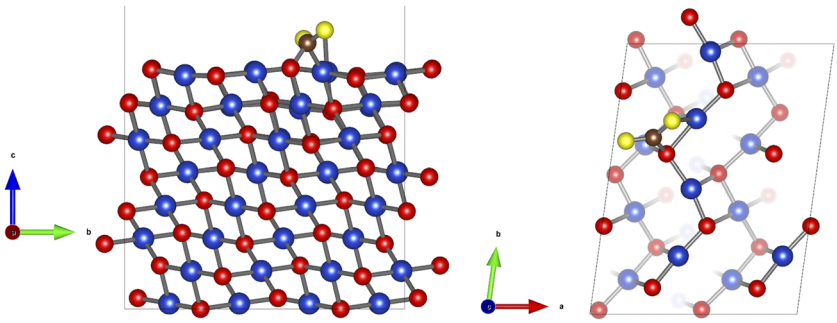

FIG. 4. Representation of one of the relaxed complete systems. Left: side view; right: top view. Blue and red spheres represent Cu and O atoms, respectively, while O and C atoms of the CO_2 molecule are represented by yellow and brown spheres, respectively.

5. Calculating adsorption energy

After calculating the final energies of the steps explained above, the chemisorption energy of the CO_2 molecule has been calculated from the relation below to find the surface with the strongest adsorption,

$$E_{ads} = E_{surf+CO_2} - (E_{surf} + E_{CO_2}). \quad (1)$$

Based on this definition, negative and positive adsorption energies specifiy an exothermic and endothermic adsorption process, respectively.

Ideally, a high performance adsorbent adsorbs the CO_2 molecules with the adsorption energies in a range of 40–80 kJ/mol.[41] Based on these criteria, a major objective of DFT calculations is to find a higher-performance surface between these two surfaces.

B. MD modeling

A Large-scale Atomic/Molecular Massively Parallel Simulator (LAMMPS) molecular dynamics simulator has been used to evaluate the rheological SC-CO_2 fluid properties.[42,43] Molecular modeling of SC-CO_2 fluid is challenging and requires a careful treatment due to the fairly weak intermolecular interactions. Therefore, to conduct atomistic simulations of SC-CO_2, it is really crucial to apply a generic and accurate force field. Several models have been proposed so far to capture the thermodynamic behavior of the SC-CO_2 liquid;[44–46] however, some of them underestimate the inter-molecular forces in condensed phases. In this study, the COMPASS force field, as one of the most reliable models which provides an accurate inter-atomic and inter-molecular interactions, especially in condensed phases,[11] has been applied for SC-CO_2 modeling in different temperatures and pressures. In this force field, the total energy is calculated by the contributions of bond stretching, angle deformation, cross-coupling of bond-bond and bond-angle, and non-bonded interactions including the electrostatic and van der Waals (vdW) terms. All the parameters required for the force field can be found in the paper published by the developer of COMPASS.[11]

The system including pure SC-CO_2 has been carefully examined with the experimental thermo-physical parameters. The unit cell with the cell dimensions of 10 nm is initially filled with CO_2 molecules with different densities depending on the phase behavior parameters (i.e., temperature and pressure).

Charge-group-based cutoffs are applied for the calculation of the non-bonded interactions for both vdW and electrostatic terms. The particle-particle particle-mesh (pppm) solver[47] is applied at each time step to compute long-range Coulombic interactions. The tail corrections are also added for the vdW interactions using neutral groups.[48] The cut-off values are usually in a range of 9.0 and 10.0 Å in the cases.

Molecular modeling of the systems including different bonding types (i.e., metallic, covalent, ionic, and vdW) is more challenging. Electron density calculation using DFT can resolve this problem, but it is quite computationally expensive for the scale of the nanostructures. Atomic-level simulations are not able to calculate the electron density variation; however, some force field potentials were developed to capture the overall effects of the electronic degrees of freedom. These force fields provide the ability for bond breaking and new bond formation without simulating the electrons themselves, for example, Tsuneyuki *et al.*,[49] Van Beest *et al.*,[50] and Tersoff[51–53] in which the charge of the Coulomb interactions are fixed. These potentials are less robust and reliable in the systems that need charge adjustment in response to changing system conditions. In order to capture the charge variation effect in these kinds of systems, some other force fields are also developed to provide a variable charge transfer scheme and form a bridge between quantum chemical and empirical force field calculations. For example, the reactive force field (ReaxFF)[54] is one of the most applicable variable charge transfer schemes; however, it cannot cover the full range of bonding types operating in a wide range of systems. Recently, a more robust and flexible reactive force field (Charge-Optimized Many-Body; COMB)[12] has been developed in which the atomic charges are allowed to change dynamically with the changing system condition and can capture the effect of the full range of bonding types.

In this study, the interaction parameters between the CuO NP and CO_2 molecules have been modeled using the COMB potential[12] that includes both charge transfer and the many-body interactions and can provide a flexibility and power for modeling the systems including the full range of bonding types. There is one cylindrical CuO NP in the systems including CO_2 molecules (see Fig. 5) under different SC conditions. Atomic structures for MD calculations have been visualized using Open VIsualization TOol (OVITO).[55] The base surface

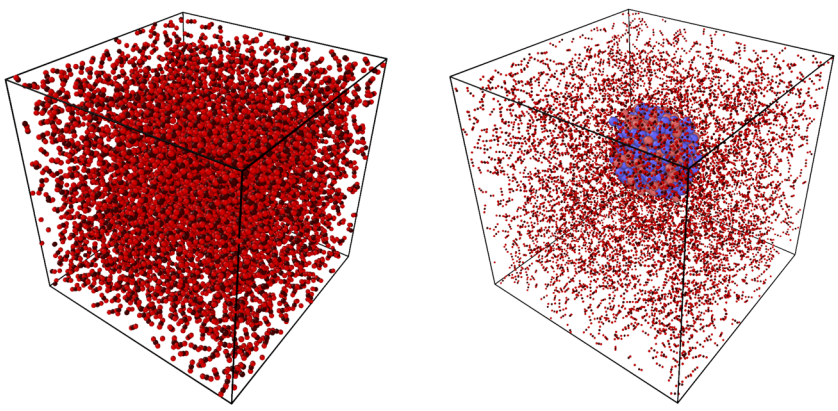

FIG. 5. Schematic of the initial state of molecular dynamics simulation. Left: Pure SC-CO_2. (Color scheme: O = red, C = dark brown). Right: CuO NP in liquid SC-CO_2. (Color scheme for CuO NP: Cu = red, O = dark brown).

TABLE II. Initial SC-CO_2 liquid density and the number of CO_2 molecules at different temperatures and pressures.

	Case #1 P = 200 bars T = 350 K	Case #2 P = 200 bars T = 410 K	Base Case P = 200 bars T = 380 K	Case #3 P = 150 bars T = 380 K	Case #4 P = 250 bars T = 380 K
Density (g/cm^3)[56]	0.61	0.35	0.46	0.31	0.55
#CO_2 molecules	15 591	8871	11 679	8022	14 022

of the CuO NP has been generated with the radius of 1 nm of the surface which has competitively stronger adsorption based on the DFT results. The height of the cylindrical NP has been considered to be 2 nm so that the base surfaces, lateral surface, and volume of the NP are 6.28 nm^2, 12.57 nm^2, and 6.28 nm^3, respectively. In order to mimic the initial volume fraction of the NP about 1%, the dimension cells has been considered to be 8.56 nm in all directions for all the cases.

The NP has been constructed with 650 copper and oxygen atoms, while a different number of CO_2 molecules have been initially applied at different SC conditions based on the experimental average-number density at the given temperature and pressure. The details are listed in Table II.

The velocity Verlet method,[57] with a 1 fs time step for the pure SC-CO_2 system and a 0.2 fs time step for the SC-CO_2 system including the CuO NP, has been applied as the integrator in all simulations.

In all the cases, first, the system has been pre-equilibrated for 150 ps at the desired temperature by carrying out the isothermal NVT canonical ensemble for the system of atoms initially arranged in a perfect structure lattice. Second, the isothermal-isobaric NPT ensemble has been carried out at the desired temperature and pressure. This ensemble has been applied for 150 ps and 500 ps, respectively, for the pure SC-CO_2 system and the system including the CuO NP in order to reach the equilibrium thermodynamic state. Then, the average densities and thermo-physical properties (i.e., viscosity and diffusion) of the systems are calculated by averaging over 200 ps trajectory. The methods used to calculate viscosity and diffusion have been explained below.

1. Viscosity

The Green-Kubos (GK) formula[58] has been used to calculate the shearing viscosity of the system in which the viscosity can be related to the correlation functions of the corresponding tensor in thermal equilibrium. In the GK formula, first, the stress autocorrelation function [SAFC; $C_\eta(t)$] is calculated as follows:

$$C_\eta(t) = \left\langle \sum_{x<y} P_{xy}(t) P_{xy}(0) \right\rangle. \quad (2)$$

P_{xy} refers to an independent component of the stress in the xy direction; however, there are other off-diagonal components of the stress tensor (i.e., P_{xz} and P_{yz}) that are used for the shear viscosity calculation. The brackets $\langle \ldots \rangle$ denote an average over an equilibrium ensemble. Then, the viscosity is calculated by the integration of SAFC over time,

$$\eta = \frac{V}{K_B T} \int_0^\infty C_\eta(t) dt, \quad (3)$$

where η is the viscosity and V, T, and K_B are the volume of the system, temperature in Kelvin, and the Boltzmann constant, respectively.

2. Self-diffusion coefficient

The self-diffusivity is different from the transport-diffusivity. The self-diffusivity describes the random motion of a molecule in the absence of any gradients that would cause a mass flux. The self-diffusion coefficient (D) of the systems is calculated using the Einstein relation[59] as follows:

$$D = \frac{1}{6} \lim_{t \to \infty} \frac{d}{dt} \left\langle (r_i(t) - r_i(0))^2 \right\rangle, \quad (4)$$

where $r_i(t)$ is the position of the center of mass of the molecules i at time t, $r_i(0)$ is the initial position, and $\langle (r_i(t) - r_i(0))^2 \rangle$ indicates an ensemble average which is the mean square displacement (MSD). According to Eq. (2), the slope of the MSD is proportional to the diffusion coefficient of the diffusing atoms in the canonical ensemble. So, by taking the slope of the trajectories of the line of calculated MSD over the averaging period, the diffusion coefficient has been calculated. The calculated MSD as a function of time together with the fit to the Einstein relation for the Base Case (as an example) system including pure SC-CO_2 liquid and SC-CO_2 based nanofluid is discussed in Appendix B.

Indeed, the self-diffusion coefficient is a parameter that would be affected with the system-size effects and this coefficient must be corrected for the system-size effects; however, relatively few MD studies take this into consideration. The system-size effects on the accurate calculation of the self-diffusion coefficient would not be crucial for the relative large system sizes (i.e., more than 1000 molecules) or bigger cut-off radii of the force field potential. In the current study, the system-size effects on the self-diffusion coefficient have been evaluated and the results showed that the system size considered is large enough to avoid affecting the self-diffusion coefficient calculation.

III. RESULTS AND DISCUSSION

In Sec. II, the details of the computation methodology are described. In this section, the results of the study have been explained.

A. *Ab initio* QM (DFT) modeling

As stated, three different possible magnetic orderings of the atoms in the surfaces (i.e., bulk-like, line-by-line, and layer-by-layer) have been investigated to calculate the energy of the optimized surfaces (E_{surf}). The results of the surface energies with the three different magnetic orderings show that these two surfaces [i.e., (011) and (111)] are most stable in the bulk-like magnetic ordering, so this magnetic ordering has been applied for the chemisorption energy calculations. The results of the surface energies with the three different magnetic orderings show that these two surfaces are most stable in the bulk-like magnetic ordering, so this magnetic ordering has been applied for the chemisorption energy calculations. The results show that the CuO(111) surface with a calculated surface energy of 0.76 J/m^2 is more stable than the CuO(011) surface with a surface energy of 0.94 J/m^2.

As discussed earlier, the CO_2 adsorption has been studied by placing the molecule on top of the atomic sites of the surfaces, parallel and perpendicularly, with different possible directions. The results of DFT show that the CO_2 molecule repels from the surface when it is placed perpendicularly to the O sites of the surfaces or close to the Cu sites with every direction. However, it binds to the O sites of the surfaces, exothermically and endothermically, when it is placed parallel to the surface on top of these sites.

Generally, the results show that the (011) surface has comparatively stronger adsorption than the (111) surface. Different bindings and chemisorption energies calculations on the (011) and (111) surfaces are explained in the following, respectively.

1. CuO(011) surface

As shown earlier in Fig. 4, there are two oxygen (one of them is upper) and two copper atoms in the top layer. The results show that the strongest binding is created by placing the CO_2 molecule parallel to the surface in the y-direction on the upper O atoms on the surface (configuration A) with the adsorption energy of −99.06 kJ/mol (see Fig. 6) (exothermic adsorption).

The second strongest binding is created by placing the CO_2 molecule parallel to the surface in the x- and y-directions on the lower O atoms on the surface (configuration B) with the adsorption energy of −86.1 kJ/mol (see Fig. 7) (exothermic adsorption.)

The third strongest binding is created by placing the CO_2 molecule parallel to the surface in the x-direction on the upper O atoms on the surface (configuration C) with the adsorption energy of −61.7 kJ/mol (see Fig. 8) (exothermic adsorption).

2. CuO(111) surface

As discussed earlier, the CuO(111) surface also consists of two oxygen (one of them is upper) and two copper atoms in the top layer (see Fig. 4). The strongest binding is created when the CO_2 molecule is placed parallel to the surface in the x- and y-directions on the upper O atoms on the surface (configuration A) with the adsorption energy of −76.2 kJ/mol (see Fig. 9) (exothermic adsorption).

The second strongest binding is created by placing the CO_2 molecule parallel to the surface in the y-direction on the lower O atoms on the surface (configuration B) with the adsorption energy of 24.1 kJ/mol (see Fig. 10) (endothermic adsorption).

The third strongest binding is created by placing the CO_2 molecule parallel to the surface in the x-direction on the lower O atoms on the surface (configuration C) with the adsorption energy of 11.9 kJ/mol (see Fig. 11) (endothermic adsorption).

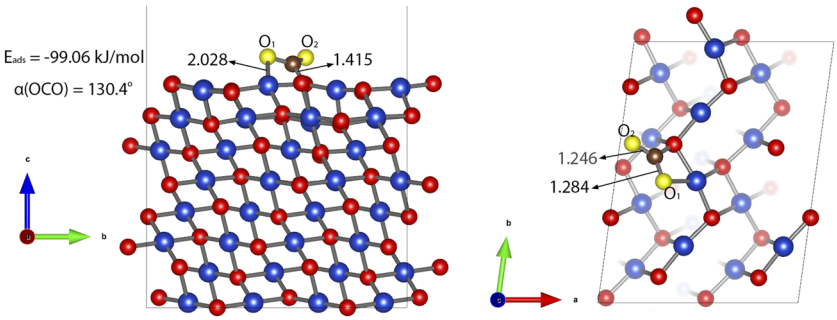

FIG. 6. Optimized adsorption configuration of the CO_2 molecule on CuO(011) for configuration A. Left: side view; right: top view. Blue and red spheres represent Cu and O atoms, respectively, while O and C atoms of the CO_2 molecule are represented by yellow and brown spheres.

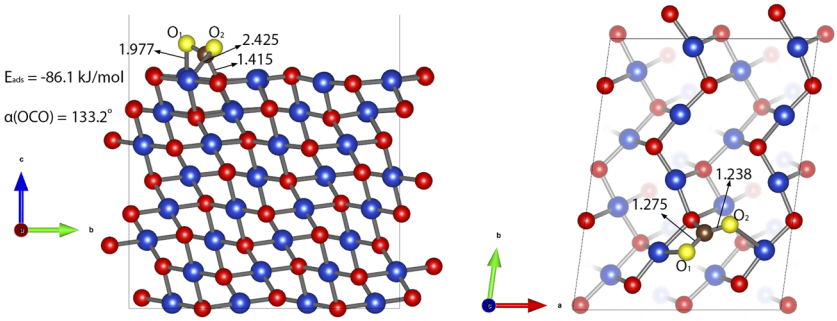

FIG. 7. Optimized adsorption configuration of the CO_2 molecule on CuO(011) for configuration B. Left: side view; right: top view. Blue and red spheres represent Cu and O atoms, respectively, while O and C atoms of the CO_2 molecule are represented by yellow and brown spheres.

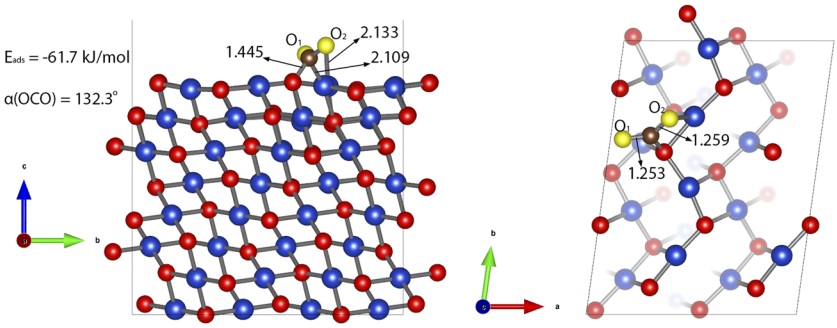

FIG. 8. Optimized adsorption configuration of the CO_2 molecule on CuO(011) for configuration C. Left: side view; right: top view. Blue and red spheres represent Cu and O atoms, respectively, while O and C atoms of the CO_2 molecule are represented by yellow and brown spheres.

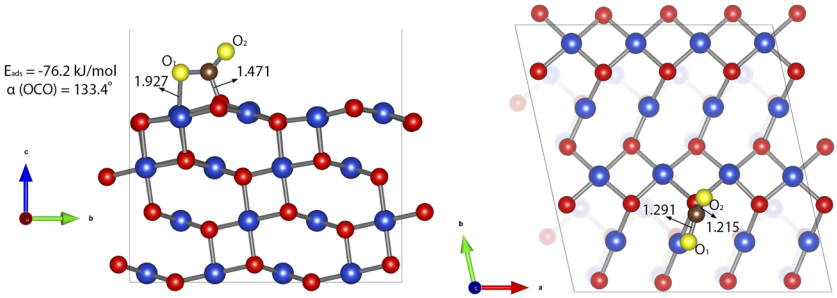

FIG. 9. Optimized adsorption configuration of the CO_2 molecule on CuO(111) for configuration A. Left: side view; right: top view. Blue and red spheres represent Cu and O atoms, respectively, while O and C atoms of the CO_2 molecule are represented by yellow and brown spheres.

The results of DFT calculation show a significant structural change in the CO_2 molecule and energy adsorption with different configurations on the CuO(011) and CuO(111) surfaces. The energies of adsorption and geometrical parameters are summarized in Table III.

Long-range dispersion forces have been taken into account with the electron correlations for the long-range interactions that are responsible for vdW forces and are required for the accurate description of the interactions between the CO_2 molecule and CuO surfaces. In order to highlight the importance of applying vdW forces, the chemisorption energies have also been calculated without considering vdW forces (see Table S1 in the supplementary material).

As stated earlier, the adsorption energies of CO_2 in a range of 40–80 kJ/mol[41] are ideal for a high-performance adsorbent. Based on the results calculated, the CuO(011) clearly and more strongly adsorbs the CO_2 molecules than the CuO(111). Therefore, the CuO NP has been constructed with the cross sections that provide the CuO(011) surface.

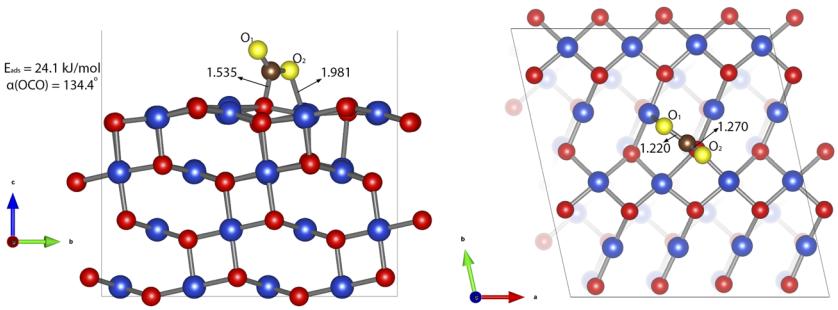

FIG. 10. Optimized adsorption configuration of the CO_2 molecule on CuO(111) for configuration C. Left: side view; right: top view. Blue and red spheres represent Cu and O atoms, respectively, while O and C atoms of the CO_2 molecule are represented by yellow and brown spheres.

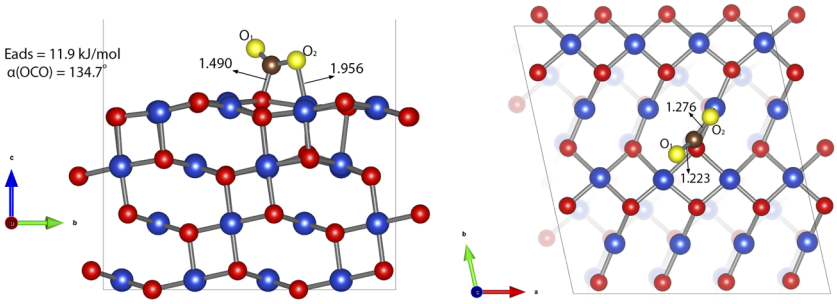

FIG. 11. Optimized adsorption configuration of the CO_2 molecule on CuO(111) for configuration B. Left: side view; right: top view. Blue and red spheres represent Cu and O atoms, respectively, while O and C atoms of the CO_2 molecule are represented by yellow and brown spheres.

TABLE III. Adsorption energies and representative geometrical parameters of a CO_2 molecule adsorbed at the (011) and (111) surfaces of CuO.

Surface	Bonding type	E_{ads} (kJ/mol)	d(C–O_1) (Å)	d(C–O_2) (Å)	α(OCO) (deg)	d(C–O_{SURF}) (Å)	d(O_1–Cu_{SURF}) (Å)	d(O_2–Cu_{SURF}) (Å)
CO_2 (gas phase)		...	1.176	1.176	180	...	...	...
(011)	Config. A	–99.1	1.280	1.246	130.4	1.415	2.028	...
	Config. B	–86.1	1.275	1.449	133.2	1.415	1.977	2.425
	Config. C	–61.7	1.253	1.259	132.3	1.445	1.253	1.259
(111)	Config. A	–76.2	1.291	1.215	133.4	1.471	1.927	...
	Config. B	24.1	1.220	1.270	134.4	1.535	...	1.981
	Config. C	11.9	1.223	1.276	134.7	1.490	...	1.956

B. MD modeling

In this section, first, the density, viscosity, and diffusion of the system including the pure SC-CO_2 calculated from MD simulations have been compared with the results obtained from the literature and experimental studies in order to validate the procedure of modeling. Second, these properties have also been evaluated for the SC-CO_2 system including the CuO NP in different thermodynamic conditions to study the effect of the CuO NP on the rheology properties of SC-CO_2.

The fundamental characteristics of aggregation and the population density between the atoms in a system can be analyzed by calculating the probability of finding a particle versus the distance from another particle. The radial distribution function (RDF) which is a useful tool to describe the structure of a system would provide this capability.

The intermolecular C–O pair correlation function for the SC-CO_2 liquid system calculated at different thermodynamic conditions in this study has been compared with the work of Aimei *et al.*[60] in Fig. 12. The essential features of the pair correlation functions are the position of the first peak and minimum. As can be seen, these features of the calculated RDF are in excellent agreement with those of Ref. 60. The first neighbor C–O distance is around 4.1 Å, and the first minimum is around 6.1 Å. The deviation between the results is mainly due to the different thermodynamic conditions.[61]

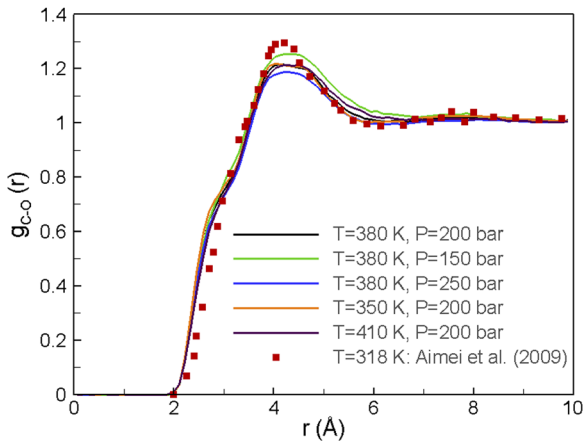

FIG. 12. A comparison between the radial distribution function of C–O calculated for the SC-CO_2 liquid system in this study at different thermodynamic conditions and the one presented at 318 K by Aimei *et al.*[60]

Figure 13 shows the results of the calculated density of the isothermal and isobaric pure SC-CO_2. The calculated densities are compared with experimental data,[56] and as can be seen, the agreement between these two data sets is excellent.

Figure 14 shows the results of the calculated viscosity of the isothermal and isobaric pure SC-CO_2. The calculated viscosity has been compared with the correlation equation developed by Fenghour *et al.*[62] The calculated viscosity shows a similar trend with the correlation equation which is increased with pressure and is decreased with temperature. However, there is a slight deviation between them, which might be observed for the viscosity calculation by atomistic scale modeling. This is mainly because of the time correlations between the stress tensors at varying time intervals and time integration of the correlation data over a long time.

To the best of our knowledge, there were no experimental values for the self-diffusion coefficient in the conditions examined in this study. However, there were experimental measurements in other conditions. Figure 15 compares the self-diffusion coefficient of the SC-CO_2 calculated with the COMPASS force field employed in this study and the experimental studies performed by Etesse *et al.*[63] and Groβ *et al.*[64] The self-diffusion coefficient of the SC-CO_2 was measured at the two isotherms 323 and 348 K at pressures ranging from 100 to 500 bars. It was also measured at 373 K in the pressure range from 300 bars to the top. The self-diffusion values calculated in this study show a very excellent agreement with the trend of the measured values.

After the validation of employing the COMPASS force field potential for the SC-CO_2 modeling and the procedure of the viscosity, density, and self-diffusion coefficient calculations, the CuO NP described above has been added to the system. The COMB force field potential has been employed for the interaction of the NP and CO_2 molecules, as stated earlier.

Figure 16 shows the adsorption of the CO_2 molecules by the CuO NP at the end of the simulation for the Base Case (as an example). In this figure, a mono-layer of adsorbed CO_2 molecules on the surface of the NP can be clearly seen.

As mentioned earlier, RDF would provide the agglomeration and diffusion status of the system. Figure 17 shows the intermolecular pair correlation functions for Cu–C of the NP and CO_2 molecules. This would be helpful for more comprehensively understanding the aggregation and bonding distance

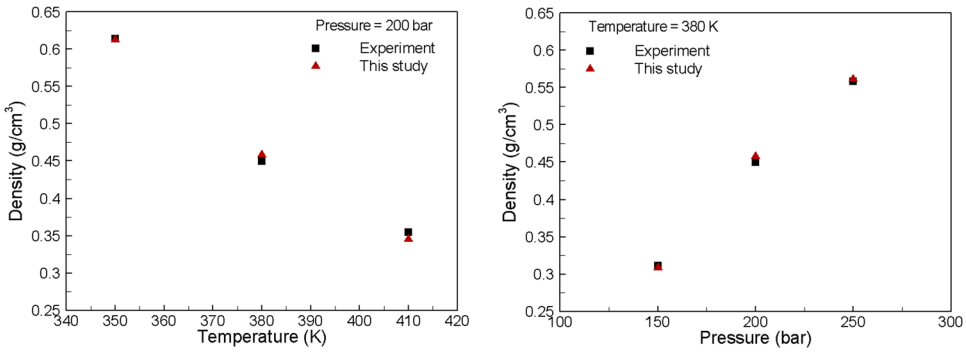

FIG. 13. A comparison between the densities of the SC-CO_2 liquid simulated with COMPASS potential in this study at different temperatures (left) and pressures (right) and those measured with the experiment.[56]

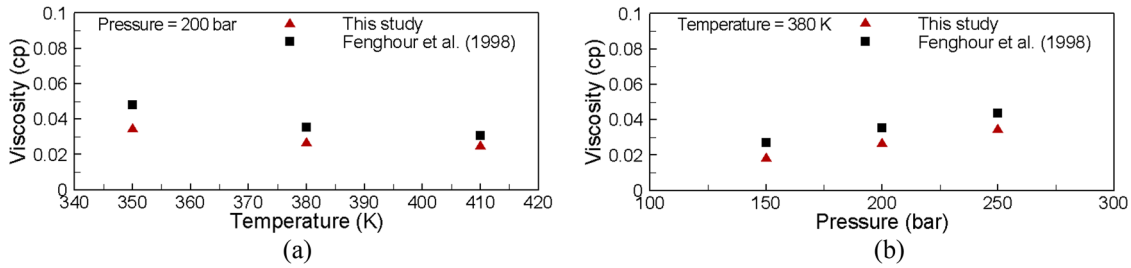

FIG. 14. A comparison between the viscosities of the SC-CO_2 liquid simulated with COMPASS potential in this study at different temperatures (a) and pressures (b) and those calculated by the correlation equation developed by Fenghour *et al.*[62]

between the CuO NP and CO_2 molecules during interaction kinetics at different thermodynamic conditions. It is worth nothing that the results here are the average of the probability of finding the C atoms versus distance from all the Cu atoms included in the NP and are not only for the Cu atoms of the NP surface.

The results show the first neighbor Cu–C distance around 2.15 Å and the minima around 2.37 for all the conditions. Then, the second peak which is larger occurred around 2.48 Å and is followed by the minima between 2.7 and 2.8 Å. It can also be seen that the relative density of the CO_2 molecules to the average density of the system at 10 Å distance from the NP is converged between 2.59 and 3.63. This is 2.59 at 250 bars and 3.63 at 150 bars. This clearly shows the aggregation of the CO_2 molecules around the CuO NP at different thermodynamic conditions which is higher at lower pressures. There is a minor difference between these values at different temperatures.

The results of the relative self-diffusion coefficient and the viscosity of the CuO NP-CO_2 system to the reference CO_2 system are shown in Fig. 18.

The variation of the relative viscosity with temperature at 200 bars shows that CuO NP has a greater impact on the enhancement of the viscosity of the reference CO_2 at higher temperatures. As can be seen, it is enhanced almost 1.3, 1.5, and 1.8 times at 350, 380, and 410 K, respectively. However, Fig. 14(a) shows that the viscosity of the reference CO_2 system decreases with temperature.

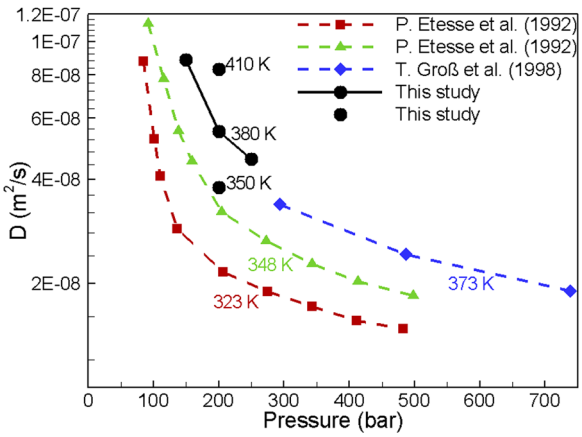

FIG. 15. A comparison between the self-diffusion coefficient of the SC-CO_2 liquid simulated with COMPASS potential in this study and those measured with experiment: (a) 323 K (Etesse *et al.*[63]), (b) 348 K (Etesse *et al.*[63]), and (c) 373 K (Groβ *et al.*[64]).

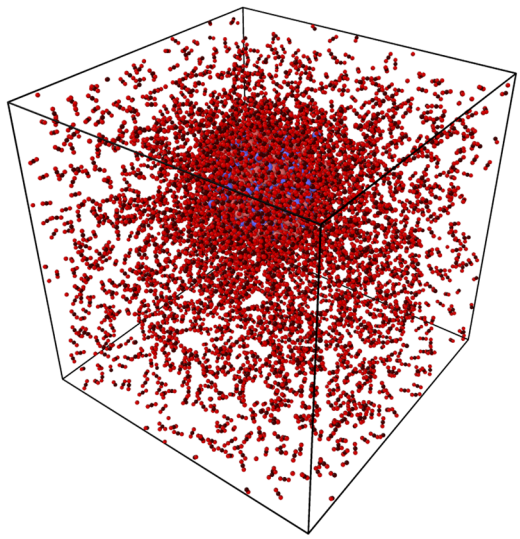

FIG. 16. Schematic of the last state of molecular dynamics simulation of a CuO NP in liquid SC-CO_2. (Colour scheme for the CO_2 molecule: O = red, C = dark brown, and for CuO NP: Cu = red, O = dark brown).

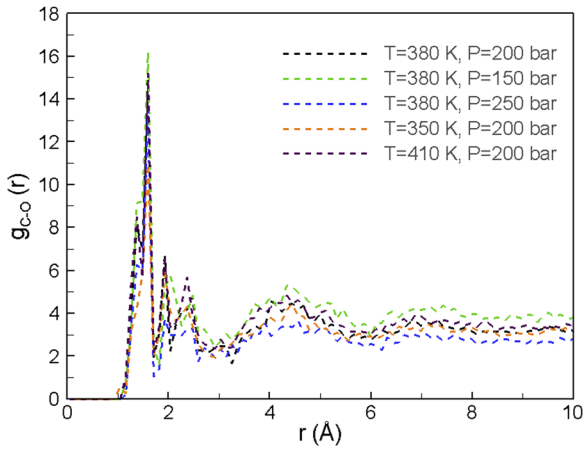

FIG. 17. Radial distribution function for the SC-CO_2 based nanofluid simulated in this study at different conditions.

The self-diffusion coefficient is a fundamental transport property which is required for understanding the thermophysical behavior (e.g., viscosity) of SC-CO_2. The diffusion coefficient describes the capacity of atoms to diffuse into other atoms; accordingly, this would help examine the viscosity as well as the agglomeration condition existing in the system with different thermodynamic conditions. The results of the pure SC-CO_2 (Fig. 15) illustrate that the diffusion coefficient is increased with temperature because of the molecular collision and random harmonic motion between the molecular bonds that dominate the excitation of atoms, which leads to an increase in the kinetic energy of the system that augments the molecular movement. This is completely what we expected based on the thermodynamic rules.

In the system including the NP, the dependency of the relative self-diffusion coefficient to the temperature in Fig. 18(a) illustrates again the relative viscosity enhancement with temperature. However, the results surprisingly show that the relative self-diffusion coefficient, which describes the ability of a CO_2 molecule movement among the other molecules in the system, is decreased with temperature at the same pressure. This confirms that the NP could attract CO_2 molecules around it and prevent them from diffusing into each other. In fact, the results of the relative viscosity and the self-diffusion coefficient suggest that the fluid properties are highly enhanced with temperature by the CuO NP.

Despite the direct relation of the relative self-diffusion and viscosity with temperature at 200 bars, it has not been observed with pressure at 380 K. As can be seen in Fig. 18(b), the relative viscosity is almost enhanced 2.5 times at 150 bars and then this enhancement is decreased to 1.5 times at 200 bars and again is increased to almost 2.1 times at 250 bars. However, it is worth noting that the viscosity for the pure SC-CO_2 system is enhanced in a direct relation with pressure [see Fig. 14(b)]. This unclear trend for the relative self-diffusion coefficient and the relative viscosity enhancement might be due to the changing parametric conditions and the volume fraction of the NP. The transport coefficients of the nanofluid depend not only on the NP size and material but also on the volume fraction of the NP so that the viscosity would enhance more with the volume fraction of the NP.

The results of the relative self-diffusion coefficient show again an opposite trend with the relative viscosity, which is a confirmation for the calculated relative viscosity.

The isothermal-isobaric ensembles (NPT) in which the number of atoms (N), pressure (P), and temperature (T) are fixed in the system are the most important and complex ensembles that are applied in this study to have a system with the desired thermodynamic conditions. In this ensemble, the volume of a system must be allowed to fluctuate in order to maintain a fixed internal pressure. Then, we may view an isobaric system that is compressed or expanded uniformly in response to instantaneous internal pressure fluctuations such that the average internal pressure is equal to an external applied pressure.

It is worth noting that the results (Fig. 19) show that the volume fraction is varied between 0.9 and 1.0 in all equilibrium thermodynamic states studied. It can be seen that the volume fraction of the NP is not maintained constant at different thermodynamic states due to the change in the volume of the simulation box in order to fix the pressure of the system. This is mainly because different amounts of CO_2 molecules are adsorbed around the NP under different thermodynamic conditions which leads to the compression of the total volume of the system at the final equilibrated pressure. The pressure reached the equilibrium and desired value in all cases before calculating the thermodynamic properties.

The results show a direct trend with temperature [see Fig. 19(a)] so that it is increased from 0.9 at 350 K to 0.96 at 410 K; however, it is not seen with pressure [see Fig. 19(b)].

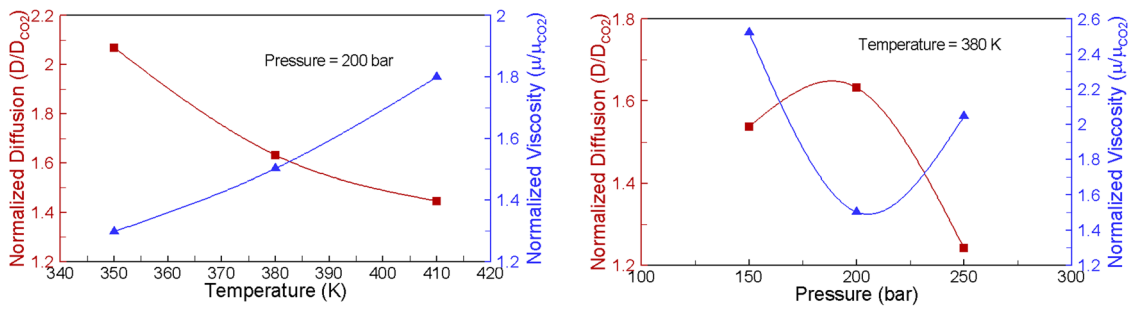

FIG. 18. Normalized self-diffusion coefficient (red lines) and normalized viscosity (blue lines) of the CO_2 based nanofluid at different temperatures (a) and pressures (b).

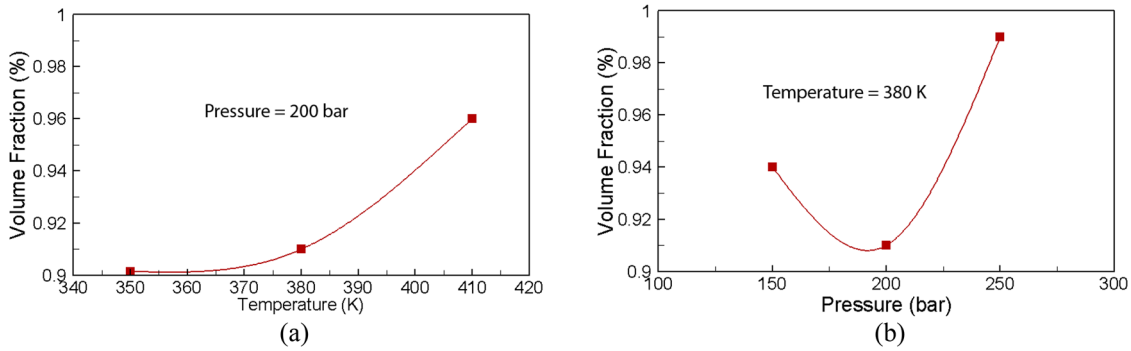

FIG. 19. Volume fraction of the NP at equilibrium thermodynamic state of different temperatures (a) and pressures (b).

As can be seen in Fig. 19(b), the volume fraction of the NP is 0.94 at 150 bars and then is decreased to 0.91 at 200 bars and again to 0.99 at 250 bars. For having this manner of change, it is worth noting that the ability of the NP for CO_2 molecule adsorption would change with thermodynamic conditions, and what we observe is that the total volume of the system is more compressed in P = 200 bars; however, it is not that significant compared to P = 150 bars.

IV. CONCLUSIONS

The present study elucidates the idea of calculating the rheological properties of super critical CO_2 with CuO NP using a multi-scale computational framework. Nanofluids are fundamentally characterized by the fact that Brownian agitation overcomes any settling motion due to gravity. Undesirably, particle collision can lead to the agglomeration process whereby large, sometimes up to micron-sized, particles are produced. Thus, a stable nanofluid is possible as long as van der Waals interactions between NPs are decreased. For stable nanofluids, the repulsive forces between particles must be dominant, and this would be provided by a stronger monolayer of adsorbed CO_2 molecules on the surface of the NP which is the most crucial factor in the formation of a stable nanofluid.

For selection of the most appropriate NP composition to develop a stable nanofluid, first, we studied the bulk CuO properties such as lattice constants, bandgaps, and magnetic moments based on the DFT+U methodology. Second, we studied the interaction of CO_2 molecules with two different CuO surfaces [i.e., (011) and (111)] by solving the quantum mechanics equations of the electronic structures at absolute zero. Next, we have performed analyses of the geometries and electronic properties of CO_2 adsorption on the surfaces of CuO, with a correction for the long-range dispersion interactions. The results show that the CO_2 molecule is adsorbed more strongly on the (011) surface with an adsorption energy of −99.06 kJ/mol compared to the (111) surface. These calculations provide useful information to make CuO NPs where the CO_2 adsorption is maximum.

Then, a computational methodology based on the MD is used to evaluate the rheological properties of the nanofluid in different thermodynamic states. The pure SC-CO_2, first, has been modeled by employing the COMPASS force field potential. The results of the density, viscosity, and self-diffusion show excellent agreement with the literature and experimental values. In the following, the SC-CO_2 based nanofluid has been modeled in order to study the effect of the CuO NP with the volume fraction of 1% on the enhancement of the fluid properties. The COMB force field potential is employed for simulating the CuO NP and the interaction between the CO_2 molecules and the NP surface. This potential is a variable charge force field and contains many-body effects that allow for the breaking of the existing bonds and the formation of new bonds. The COMPASS force field potential is also employed for the interactions between CO_2 molecules. The combination of these potentials is quite a new approach for the study of the SC-CO_2 based nanofluid. The results show that the viscosity of the SC-CO_2 is enhanced between 1.3 and 2.5 times under the conditions studied by adding the CuO NP. These methodologies applied in this study can be used for studying the rheological properties of the SC-CO_2 based nanofluid carrying other metal oxides such as TiO_2 and Al_2O_3.

SUPPLEMENTARY MATERIAL

See supplementary material for calculated chemisorption energy of a CO_2 molecule at the (011) and (111) surfaces of CuO with and without taking into account the long-range interactions of van der Waals (vdW, dispersive) forces.

ACKNOWLEDGMENTS

The authors would like to acknowledge and greatly appreciate the financial support from VISTA which is a basic research program in collaboration between the Norwegian Academy of Science and Letters, and Statoil. The authors would also like to thank the Department of Mechanical and Industrial Engineering at the Norwegian University of Science and Technology (NTNU). The authors also acknowledge generous grants of high performance computer time from both Vilje and UNINETT Sigma.

APPENDIX A: PLANEWAVE CUTOFF ENERGY AND k-POINT GRID CONVERGENCE FOR THE CuO BULK STRUCTURE

Since the total energy of the system is a function of the planewave cutoff energy and the k-point grid, these computational tools must be converged to calculate accurate results.

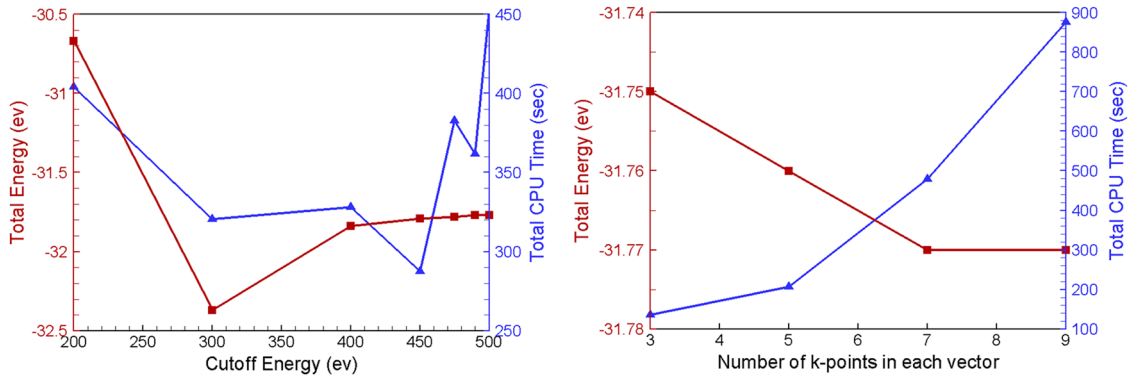

FIG. 20. Left: planewave cutoff energy; right: k-point grid convergence for the CuO bulk structure.

Generally, the larger amount of the planewave cutoff energy and the higher number of sampled points lead to more accurate results; however, the computational cost will increase drastically, especially by increasing the number of k-points. For this reason, balancing of the convergence with the computational cost has been attempted. Here, the results of the planewave cutoff energy and k-point grid convergence for CuO bulk structure have been shown in Fig. 20.

APPENDIX B: SELF-DIFFUSION COEFFICIENTS CALCULATED FROM MOLECULAR DYNAMICS SIMULATION

As stated in the paper, the self-diffusion coefficient can be calculated from molecular dynamics simulation. The procedure of the calculation is to take a slope of the trajectories of the line of the calculated MSD over the averaging period. Here, the slope lines fitted to the calculated MSD as a function of time for the Base Case (as an example) system including pure SC-CO_2 liquid and SC-CO_2 based nanofluid are shown in Fig. 21. The start time of the averaging period is shifted to zero. The same procedure has been applied for the other conditions of temperature and pressure to calculate this coefficient.

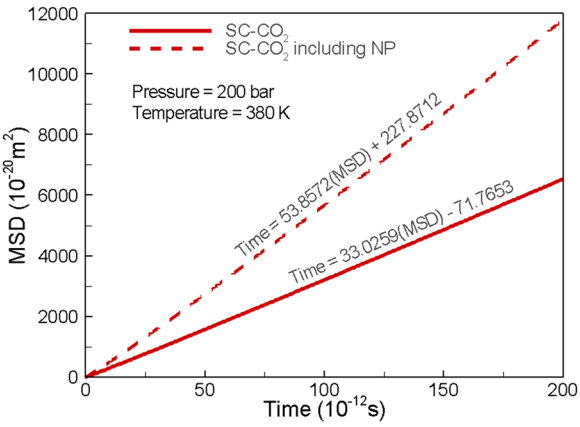

FIG. 21. The fitting results to the Einstein relation for the self-diffusion coefficient calculation as a function of time for the Base Case system including pure SC-CO_2 liquid and SC-CO_2 based nanofluid.

[1] L. Li, Y. Zhang, H. Ma, and M. Yang, Phys. Lett. A **372**(25), 4541–4544 (2008).
[2] N. Sankar, N. Mathew, and C. B. Sobhan, Int. Commun. Heat Mass Transfer **35**(7), 867–872 (2008).
[3] C. Sun, W. Q. Lu, J. Liu, and B. Bai, Int. J. Heat Mass Transfer **54**(11-12), 2560–2567 (2011).
[4] V. Y. Rudyak and S. L. Krasnolutskii, Phys. Lett. A **378**, 1845–1849 (2014).
[5] A. Loya and G. Ren, J. Mater. Sci. **50**(11), 4075–4082 (2015).
[6] V. Y. Rudyak and A. V. Minakov, Eur. Phys. J. E **41**(1), 15 (2018).
[7] A. E. Hernández Battez, R. González Rodríguez, J. L. Viesca Rodríguez, J. E. Fernández Rico, J. M. Díaz Fernández, A. S. Machado Rodríguez, and J. A. Riba López, Wear **265**(3-4), 422–428 (2008).
[8] C. Zhao, Y. K. Chen, and G. Ren, Tribol. Trans. **56**(2), 275–283 (2013).
[9] B. Wei, Q. Li, F. Jin, H. Li, and C. Wang, Energy Fuels **30**(4), 2882–2891 (2016).
[10] A. Sorooshian, R. Ashwani, H. K. Choi, M. Moinpour, A. Oehler, and A. Tregub, MRS Online Proceedings Library Archive, 816, 2004.
[11] J. Yang, Y. Ren, A. M. Tian, and H. Sun, J. Phys. Chem. B **104**(20), 4951–4957 (2000).
[12] S. R. Phillpot and S. B. Sinnott, Science **325**(5948), 1634–1635 (2009).
[13] B. Devine, T. R. Shan, Y. T. Cheng, A. J. McGaughey, M. Lee, S. R. Phillpot, and S. B. Sinnott, Phys. Rev. B **84**(12), 125308 (2011).
[14] J. E. Jones, Proc. R. Soc. London, Ser. A **106**(738), 463–477 (1924).
[15] R. A. Buckingham, Proc. R. Soc. London, Ser. A **168**(933), 264–283 (1938).
[16] M. S. Daw and M. I. Baskes, Phys. Rev. B **29**(12), 6443 (1984).
[17] J. Tersoff, Phys. Rev. B **30**(8), 4874 (1984).
[18] D. W. Brenner, Phys. Rev. B **42**(15), 9458 (1990).
[19] G. Kresse and J. Hafner, Phys. Rev. B **47**(1), 558 (1993).
[20] G. Kresse and J. Hafner, Phys. Rev. B **49**(20), 14251 (1994).
[21] G. Kresse and J. Furthmüller, Comput. Mater. Sci. **6**(1), 15–50 (1996).
[22] G. Kresse and J. Furthmüller, Phys. Rev. B **54**(16), 11169 (1996).
[23] S. L. Dudarev, G. A. Botton, S. Y. Savrasov, C. J. Humphreys, and A. P. Sutton, Phys. Rev. B **57**(3), 1505 (1998).
[24] J. P. Perdew and A. Zunger, Phys. Rev. B **23**(10), 5048 (1981).
[25] K. Burke, J. P. Perdew, and M. Ernzerhof, Phys. Rev. Lett. **78**, 1396 (1997).
[26] J. Kitchin, *Modeling Materials Using Density Functional Theory* (Free Software Foundation, Boston, 2008).
[27] A. H. Larsen, J. J. Mortensen, J. Blomqvist, I. E. Castelli, R. Christensen, M. Dułak, E. D. Hermes *et al.*, J. Phys.: Condens. Matter **29**(27), 273002 (2017).
[28] K. Momma and F. Izumi, J. Appl. Crystallogr. **44**(6), 1272–1276 (2011).
[29] H. J. Monkhorst and J. D. Pack, Phys. Rev. B **13**(12), 5188 (1976).
[30] H. Wu, N. Zhang, Z. Cao, H. Wang, and S. Hong, Int. J. Quantum Chem. **112**, 2532 (2012).
[31] H. Wu, N. Zhang, H. Wang, and S. Hong, Chem. Phys. Lett. **568-569**, 84 (2013).
[32] L. I. Bendavid and E. A. Carter, J. Phys. Chem. C **117**, 26048 (2013).
[33] A. K. Mishra, A. Roldan, and N. H. de Leeuw, J. Chem. Phys. **145**, 044709 (2016).
[34] A. K. Mishra, A. Roldan, and N. H. de Leeuw, J. Phys. Chem. C **120**(4), 2198–2214 (2016).
[35] C. Kittel, *Introduction to Solid State Physics* (Wiley, New York, 1976).
[36] J. Ghijsen, L. V. Tjeng, J. Van Elp, H. Eskes, J. Westerink, G. A. Sawatzky, and M. T. Czyzyk, Phys. Rev. B **38**(16), 11322 (1988).

[37]J. B. Forsyth, P. J. Brown, and B. M. Wanklyn, J. Phys. C: Solid State Phys. **21**(15), 2917 (1988).
[38]M. Nolan and S. D. Elliott, Phys. Chem. Chem. Phys. **8**(45), 5350–5358 (2006).
[39]C. E. Ekuma, V. I. Anisimov, J. Moreno, and M. Jarrell, Eur. Phys. J. B **87**(1), 23 (2014).
[40]S. Grimme, J. Comput. Chem. **27**(15), 1787–1799 (2006).
[41]S. Chu and A. Majumdar, Nature **488**, 294 (2012).
[42]S. Plimpton, J. Comput. Phys. **117**(1), 1–19 (1995).
[43]See http://lammps.sandia.gov for more information about the code.
[44]K. B. Domański, O. Kitao, and K. Nakanishi, Mol. Simul. **12**(3-6), 343–353 (1994).
[45]J. G. Harris and K. H. Yung, J. Phys. Chem. **99**(31), 12021–12024 (1995).
[46]Z. Zhang and Z. Duan, J. Chem. Phys. **122**(21), 214507 (2005).
[47]R. W. Hockney and J. W. Eastwood, *Computer Simulation Using Particles* (Adam Hilger, NY, 1989).
[48]H. Sun, J. Phys. Chem. B **102**, 7338–7364 (1998).
[49]S. Tsuneyuki, M. Tsukada, H. Aoki, and Y. Matsui, Phys. Rev. Lett. **61**(7), 869 (1988).
[50]B. W. H. Van Beest, G. J. Kramer, and R. A. Van Santen, Phys. Rev. Lett. **64**(16), 1955 (1990).
[51]J. Tersoff, Phys. Rev. B **38**(14), 9902 (1988).
[52]J. Tersoff, Phys. Rev. B **37**(12), 6991 (1988).
[53]J. Tersoff, Phys. Rev. B **39**(8), 5566 (1989).
[54]A. C. Van Duin, A. Strachan, S. Stewman, Q. Zhang, X. Xu, and W. A. Goddard, J. Phys. Chem. A **107**(19), 3803–3811 (2003).
[55]A. Stukowski, Modell. Simul. Mater. Sci. Eng. **18**(1), 015012 (2009).
[56]R. Span and W. Wagner, J. Phys. Chem. Ref. Data **25**(6), 1509–1596 (1996).
[57]L. Verlet, Phys. Rev. **159**(1), 98 (1967).
[58]R. Kubo, J. Phys. Soc. Jpn. **12**(6), 570–586 (1957).
[59]M. P. Allen and D. J. Tildesley, *Computer Simulation of Liquids* (Oxford University Press, New York, 1987), Vol. 385.
[60]Z. H. U. Aimei, X. Zhang, L. I. U. Qinglin, and Q. Zhang, Chin. J. Chem. Eng. **17**(2), 268–272 (2009).
[61]M. Darbandi, R. Khaledialidusti, M. Abbaspour, H. R. Abbasi, and G. Schneider, in *ASME 2011 9th International Conference on Nanochannels, Microchannels, and Minichannels* (American Society of Mechanical Engineers, 2011), pp. 277–282.
[62]A. Fenghour, W. A. Wakeham, and V. Vesovic, J. Phys. Chem. Ref. Data **27**, 31 (1998).
[63]P. Etesse, J. A. Zega, and R. Kobayashi, J. Chem. Phys. **97**, 2022 (1992).
[64]T. Groß, J. Buchhauser, and H.-D. Lüdemann, J. Chem. Phys. **109**, 4518 (1998).